Button Erik S. (Orcid ID: 0000-0001-5153-6022)

Separating N_2O production and consumption in intact agricultural soil cores at different moisture contents and depths

N_2O processes in soil cores at varying depths

Erik S. Button[a], Karina A. Marsden[a], Philip D. Nightingale[b], Elizabeth R. Dixon[c], David R. Chadwick[a], David L. Jones[a,d], Laura M. Cárdenas[c*]

[a] *School of Natural Sciences, Bangor University, Bangor, Gwynedd, LL57 2UW, UK*

[b] *Plymouth Marine Laboratory, Prospect Pl, Plymouth, Devon, PL1 3DH, UK*

[c] *Rothamsted Research North Wyke, Okehampton, Devon, EX20 2SB, UK*

[d] *Centre for Sustainable Farming Systems, Food Futures Institute, Murdoch, WA 6150, Australia*

*Corresponding Author: Laura M. Cárdenas

Corresponding Author Address: Rothamsted Research North Wyke
Okehampton, Devon, EX20 2SB, UK

Corresponding Author Email: laura.cardenas@rothamsted.ac.uk

This article has been accepted for publication and undergone full peer review but has not been through the copyediting, typesetting, pagination and proofreading process which may lead to differences between this version and the Version of Record. Please cite this article as doi: 10.1111/ejss.13363

Highlights

- **How does N_2O diffusion, production and consumption vary with soil depth and soil moisture?**
- **A novel and more field-relevant system was developed to incubate intact top- and subsoil cores.**
- **Diffusion was driven by moisture and N_2O consumption and production were highest in drier soil.**
- **This new system can separate N_2O processes occurring at depth whilst replicating field conditions.**

ABSTRACT

Agricultural soils are a major source of the potent greenhouse gas and ozone depleting substance, N_2O. To implement management practices that minimise microbial N_2O production and maximise its consumption (i.e. complete denitrification) we must understand the interplay between simultaneously occurring biological and physical processes, especially how this changes with soil depth. Meaningfully disentangling these processes is challenging and typical N_2O flux measurement techniques provide little insight into subsurface mechanisms. Additionally, denitrification studies are often conducted on sieved soil in altered O_2 environments which relate poorly to *in situ* field conditions. Here, we developed a novel incubation system with headspaces both above and below the soil cores and field-relevant O_2 concentrations to better represent *in situ* conditions. We incubated intact sandy clay loam textured agricultural topsoil (0-10 cm) and subsoil (50-60 cm) cores for 3-4 d at 50% and 70% water-filled pore space (WFPS), respectively. ^{15}N-N_2O pool dilution and an SF_6 tracer were injected below the cores to determine the relative diffusivity and the net N_2O emission and gross N_2O emission and consumption fluxes. The relationship between calculated fluxes from the below and above soil core headspaces confirmed that the system performed well. Relative diffusivity did not vary with depth, likely due to the preservation of preferential flow pathways in the intact cores. Gross N_2O emission and uptake also did not differ with depth but were higher in the drier cores, contrary to expectation. We speculate this was due to aerobic denitrification being the primary N_2O consuming process and simultaneously occurring denitrification and nitrification both producing N_2O in the drier cores. We provide further evidence of substantial N_2O consumption in drier soil but without net negative N_2O emissions. The results from this study are important for the future application of the ^{15}N-N_2O

pool dilution method and N budgeting and modelling, as required for improving management to minimise N_2O losses.

Keywords: diffusion coefficient; denitrification; sulphur hexafluoride; isotope pool dilution; nitrogen cycling.

1. Introduction

Nitrous oxide (N_2O) exchange between the soil and atmosphere has received significant attention in recent decades due to its prominent role in climate change and atmospheric ozone depletion (e.g. Jia et al., 2019). More than half of global agricultural greenhouse gas emissions are from N_2O, resulting from N inputs to soil, including fertiliser and manure application (direct) and denitrification following leaching and atmospheric deposition of nitrogen (N; indirect) (Clough et al., 2005; Jia et al., 2019). There are several pathways and processes (both biotic and abiotic) that produce and consume N_2O in soils (see Butterbach-Bahl et al., 2013), however, nitrification and denitrification are widely considered the major N_2O producing processes. Under suboxic conditions, the production of atmospheric N_2O is primarily governed by microbial incomplete denitrification in the soil, where N_2O is produced from nitrate (NO_3^-) under partially anaerobic conditions (Table S1; Diba et al., 2011). Nitrification (Table S1) is an aerobic process, and some studies have shown it can be the dominant N_2O producing process (e.g. Zhang et al., 2016; Liu et al., 2016), especially where soil aeration is sufficient (35-60% water-filled pore space [WFPS]; Bateman and Baggs, 2005). However, denitrifiers are also able to consume N_2O (i.e. complete denitrification; Table S1) to produce inert dinitrogen (N_2) gas (Diba et al., 2011), which constitutes 78% of the Earth's atmosphere. Typically, N_2 is the major end product of denitrification where soil moisture is

greater than 80% WFPS (Giles et al., 2017) as it is performed by facultative anaerobic microorganisms (Butterbach-Bahl et al., 2013). This process is often masked by greater production rates and is mostly only measured when the consumption rate exceeds the production rate (i.e. net negative emissions; Chapuis-Lardy et al., 2007; Schlesinger, 2013). Measuring the consumption of N_2O directly (e.g. by N_2 flux) is challenging against a very high atmospheric background (Clough et al., 2006; Wen et al., 2016; Yang et al., 2011). In addition, the heterogeneity of N_2O processes in the soil and their measurement can lead to high error when data is scaled (Groffman et al., 2006). Accurately measuring N_2O consumption is important for modelling and prediction of future soil N budgets, for which N_2O is the most poorly constrained term, due to the abovementioned inherent challenges (Almaraz et al., 2020; Blagodatsky and Smith, 2012; Boyer et al., 2006).

The balance between gross production and consumption of N_2O in agricultural soil is complex, being influenced by a range of environmental factors (e.g., temperature, moisture, O_2 content; Chapuis-Lardy et al., 2007), soil characteristics (e.g., pH, mineral N content, porosity, organic matter content, soil depth; Clough et al., 2005; Stuchiner and von Fischer, 2022a; Chapuis-Lardy et al., 2007) and management practices (e.g., fertilizing regime, tillage, irrigation; Khalil et al., 2002; Wang et al., 2018).

The consumption of N_2O is stimulated by anaerobic conditions (high WFPS) due to the sensitivity of the metallo-enzyme, N_2O reductase, to O_2 (Richardson et al., 2009). Thus, extensively waterlogged soils, such as peat- and wetlands represent the greatest N_2O sinks globally (Schlesinger, 2013). Low mineral N contents are also thought to be important for N_2O consumption, as nitrate (NO_3^-) outcompetes N_2O as a terminal electron acceptor (Chapuis-Lardy et al., 2007). However, N_2O consumption has been found to coincide with low WFPS in both fertilized (<50% WFPS; Khalil et al., 2002) and unfertilised soil (5-20% WFPS; Wu et al.,

2013). Here, anaerobic conditions may exist in microsites heterogeneously distributed throughout the soil profile of free-draining soils, within soil aggregates (even in dry aerobic soil; Sexstone et al., 1985) or can be caused by localised respiration hot spots that deplete O_2 (Clough et al., 1999; Hill and Cardaci, 2004; Van Cleemput, 1998). Therefore, N_2O produced in the soil is not necessarily consumed in the same location but may diffuse to another site in the soil, may be lost to the atmosphere or groundwater (Shcherbak and Robertson, 2019), or become entrapped in the soil (Clough et al., 1999). In addition, aerobic consumption of N_2O is possible, where N_2O is used as an electron acceptor when NO_3^- is limited (Chapuis-Lardy et al., 2007; Wang et al., 2018). To understand these processes in a meaningful way, the physical diffusion and the gross N_2O production and consumption rates need to be separated from each other.

N_2O processes occurring deeper in the soil have received less attention but are important in understanding the balance between N_2O production and consumption (Almaraz et al., 2020; Clough et al., 2005; Jahangir et al., 2012). The movement of N_2O to the soil surface is predominantly via passive diffusion through air-filled pores in the soil. The concentration of N_2O at depth is frequently higher than near the soil surface due to lower diffusivity (Balaine et al., 2013; Currie, 1984; Davidson et al., 2004; Dong et al., 2013; Fujikawa and Miyazaki, 2005; Laughlin and Stevens, 2002; Van Bochove et al., 1998; Van Groenigen et al., 2005; Wang et al., 2018; Zona et al., 2013). This lag between production and surface emission is supported by a ^{15}N-labelled experiment by Clough et al. (1999), where it took 11 d for N_2O produced at 80 cm to first reach the soil surface and 6% remained in the soil even after 38 d (i.e. entrapment). Soil conditions restricting N_2O diffusion, thereby increasing its residence time in the soil, can increase its consumption (Chapuis-Lardy et al., 2007; Clough et al., 2005; Neftel et al., 2007). The generally higher rate of N_2O consumption and production in the topsoil is a

reflection of the greater microbial abundance and activity (Van Beek et al., 2004; van Bochove et al., 1998; Wang et al., 2018) compared to subsoils, but considerable N_2O production and consumption can also occur in the subsoil if conditions allow (Clough et al., 1999; Shcherbak and Robertson, 2019). In addition, understanding of the relation between diffusion and N_2O emissions is lacking (Balaine et al., 2013), especially in intact deep soil (Chamindu Deepagoda et al., 2019). Therefore, understanding the balance of N_2O production and consumption between topsoil and subsoil depths at different soil conditions and their relation to diffusion is needed to best predict N_2O surface emissions for modelling the global N budget (Almaraz et al., 2020; Blagodatsky and Smith, 2012; Boyer et al., 2006).

Understanding N_2O mechanisms in the soil is important for more accurate modelling and N budgeting and to support emerging attempts to minimise N_2O losses from soil. Chamindu Deepagoda et al. (2019) found a range of relative gas diffusivity rates which lowered N_2O emissions that could be monitored and maintained by land users. Stuchiner and von Fischer (2022a) recently demonstrated a case of Increased Consumption and Decreased Emissions (coined ICDE) of N_2O via promotion of anoxia from relieving the C-limitation to the microbial community.

The $^{15}N_2O$ pool dilution method is a relatively new method used by Yang et al. (2011), Yang and Silver (2016) and Wen et al. (2016, 2017) to determine the gross production and consumption of N_2O. The method, where isotopically enriched $^{15}N_2O$ is injected into a closed system and the disappearance of the label is measured over time, is currently the only method for field measurement of gross N_2O emission and uptake under undisturbed conditions (Almaraz et al., 2020). This method can also be applied to the incubation of soil cores as done by Wen et al. (2016) and Stuchiner and von Fischer (2022a), which allows for the incubation of soil cores taken from below the surface. An inherent assumption of the $^{15}N_2O$ pool dilution

method is that the $^{15}N_2O$ that diffuses into the soil mixes evenly with soil-derived N_2O. Wen et al. (2016) compared the pool dilution method with a gas-flow core method and found it to underestimate gross N_2O production and consumption. Due to the use of a closed static system in previous applications of the method, the diffusion and mixing of the labelled gas with soil pores is less likely to occur, which means the gross N_2O production and consumption may be underestimated. Therefore, a system where the mixing of the label with the soil pores is improved will result in greater accuracy of the pool dilution approach.

Here, we used a novel open dual headspace system with field-relevant O_2 concentrations to incubate intact sandy clay loam agricultural top- and subsoil cores. This system was developed to answer the question: *does the balance between soil N_2O production and consumption differ between soil depths and moisture contents in intact agricultural soil cores?* Following the ^{15}N-N_2O pool dilution (Wen et al., 2016; Yang et al., 2011) and Currie method (Currie, 1960) with SF_6 as a conservative tracer, the relative diffusivity (D_s/D_0) and the net N_2O emission and gross N_2O emission and uptake rates were measured. We hypothesised that, i) the rate of diffusion would decrease with soil depth and wetness due to greater soil density and lower porosity; ii) despite higher N_2O and lower O_2 concentrations deeper in the soil, consumption of N_2O will be greater in the more microbially-active topsoil; and iii) a WFPS above the critical level (ca. ≥60%; Bateman and Baggs, 2005) will increase N_2O consumption, whereas at a lower WFPS, N_2O consumption will be minimal.

2. Materials and methods

2.1. Soil collection and characterisation

Sandy clay loam textured freely draining arable soil was collected from Abergwyngregyn, North Wales (53°14’29”N, 4°01’15”W) in February 2020. The soil is classified as a Eutric Cambisol (WRB) or Typic Hapludalf (US Soil Taxonomy) and has a crumb

structure due to high levels of earthworm bioturbation. This soil was chosen as it is a globally extensive temperate soil type and it is common under agricultural production (WRB, 2014). Prior to collection, the field had been used for winter wheat (*Triticum aestivum*) production. Soil was collected from 6 randomly selected locations within the field from the topsoil (0 - 10 cm) and subsoil (50 - 60 cm), which were retained as 6 independent replicates. The latter soil depth was from below the plough layer and the field had no history of subsoiling. The latter depth was chosen as it was representative of the B horizon, assumed to be 'undisturbed' from mechanical soil management and provided enough distinction in soil characteristics from the topsoil cores. Two disturbed soil samples and 3 intact soil cores (using stainless steel rings of 53 mm outside diameter x 50 mm height, 104 cm^3 volume; steel from Complete Stainless Ltd., Glasgow, UK) were collected from each hole at each depth, not including spare cores used for soil characterisation. Soil cores were collected by lightly hammering in the steel rings at the appropriate soil depth and retrieving them, when the entire volume was filled, by carefully digging them out. The soil cores were then placed in plastic bags (but not sealed) in the field and stored at <5°C prior to use.

One of the set of 3 soil cores per depth and hole were removed from their metal core rings, weighed and oven-dried (105°C, 24 h) immediately after collection. Dry bulk density was determined by dividing the dry weight by the soil volume. Water-filled pore space (WFPS) was determined using the volumetric water content, particle density and bulk density, using the following equation:

$$WFPS = \frac{B_d \cdot M_c}{1 - \frac{B_d}{P_d}} \cdot 100 \quad (1)$$

Where the B_d is the dry bulk density (g cm^{-3}) and M_c is the moisture content (g g^{-1}) and their product is the volumetric water content (cm^3 cm^{-3}). P_d is the particle density, assumed at 2.65

g cm^{-3}. 1- B_d/P_d is the total porosity ($cm^3\ cm^{-3}$).

5 g replicates of soil were extracted using 0.5 M K_2SO_4 at a ratio of 1:5 (w/v) on the same day the soil was collected. These were shaken at 200 rpm for 30 mins and then centrifuged (14,000 g, 10 min). The supernatant was then removed and frozen for later ammonium (NH_4^+) and NO_3^- content determination by colourimetry, according to Mulvaney (1996) and Miranda et al. (2001), respectively, with a PowerWave XS Microplate Spectrophotometer (BioTek Instruments Inc., Winooski, VT). Dissolved organic C and N in the extracts was determined using a Multi N/C 2100/2100 analyser (AnalytikJena AG, Jena, Germany). Dissolved organic N was determined by subtracting inorganic N (NO_3^- and NH_4^+) from the total dissolved N. Soil EC and pH in water were determined in a 1:5 ratio (w/v) using a Jenway 4520 conductivity meter and a Hanna 209 pH meter (Hanna Instruments Ltd., Leighton Buzzard, UK), respectively. A summary of the initial soil properties are presented in Table 1.

2.2. Experimental system

A specialised gas-flow-soil-core incubation system (DENitrification Incubation System (DENIS); Cárdenas et al., 2003), allowing controlled environmental condition control (including O_2 concentration and temperature), was adapted for this study using custom made lids used by Boon et al. (2013). The system, with 12 large individual stainless steel chambers (2120 ml), was modified to hold 53 mm wide soil cores with a lid and septum for direct gas application and sampling from a small headspace (77.2 ml) with a 3 m (4.8 mm ID, 53.4 ml) sampling tube (Fig. 1). Details of the DENIS modification and a photograph are provided in the Supplementary Information (S1, Fig. S1).

Gas flow from O_2 and N_2 (see ratios in 2.4) cylinders into the system were adjusted via mass flow controllers (MFC) to achieve the desired flow rate and O_2 concentration, and then

split via a manifold evenly to each of the 12 incubation vessels. A valve (Fig. 1) enabled flow to be either directed to enter the large headspace below the intact soil cores ('flush mode') or to enter the small headspace on top of the intact soil cores ('flow over mode'). In both modes the gas exited via the sampling tube. The MFC was calibrated for all gases used in the experiment by measuring the flow 5 times at 10 flow rate settings with a bubble meter.

In this study, two gases were used to generate the 'flush' and 'flow over' the intact soil cores (Fig. 1): an ECD-Grade N_2 cylinder and a grade zero O_2 cylinder (BOC; Linde plc, Guildford, UK). The N_2 cylinder and a compressed air line that was used for the 'flow over mode' both had SF_6 concentrations below atmospheric levels (i.e. <10 ppt). During pilot studies, we discovered that the SF_6 concentration in the O_2 cylinder was surprisingly high (*ca.* 6 ppb), which is about three orders of magnitude greater than the concentration of atmospheric SF_6 (10.6 ppt). We, therefore, decided to use this as our source of SF_6 for the incubations.

^{15}N labelled N_2O was generated specifically for this experiment using the ammonium sulphate method described by Laughlin et al. (1997). This generates N_2O and N_2 at the same ^{15}N enrichment as the ammonium sulphate. The generated N_2O and N_2 were collected in evacuated exetainers (Labco Ltd., Lampeter, UK). N_2 was removed using the cryotrapping loops in a Sercon trace gas analyser (TG2, Sercon Ltd., Crewe, UK) so that the N_2O was trapped while the N_2 was flushed to waste. Once the N_2 had been removed, N_2O was collected in a Tedlar® gas sample bag from the outlet of the TG2. The contents of the Tedlar® bag were analysed for N_2O and N_2 concentration and enrichment using a Sercon trace gas analyser and Sercon 20:22 isotope ratio mass spectrometer (Sercon Ltd., Crewe, UK).

2.3 Soil core preparation and installation

Soil cores from both depths were brought to either 50% or 70% WFPS for the

incubation experiment. These WFPS were chosen as they are either side of the 60% WFPS threshold for N_2O production and N_2O produced is likely to be underpinned by different processes (Bateman and Baggs, 2005). Soil cores were brought to the desired weight for attaining a WFPS of 50% or 70% (n = 6 each) by adding distilled water (70% WFPS) or air-drying the approximate field moist soil (50% WFPS). To calculate the difference in moisture content (ΔM_c) for achieving for the required WFPS (50% or 70%) in the incubation, the required WFPS level ($WFPS_R$; %) was multiplied by the total pore space volume (PS_v; cm^3) as demonstrated in Equation 2. The moisture content of the core (M_{cc}; cm^3) was then subtracted from this to give the difference in soil core moisture to achieve the required WFPS.

$$\Delta M_c = \frac{WFPS_R \cdot PS_v}{100} - M_{cc} \quad (2)$$

The required water needed to reach the desired WFPS level in the cores was pipetted onto the surface of the cores 24 h before installation into the incubation system. Where this water did not immediately infiltrate it was done in stages so all the water was pipetted and it did not run down the sides of the core. Cores that needed WFPS levels reducing were air dried and subsequently adjusted with additional water if they overshot the target (as described above). Cores that had not lost enough weight after air-drying overnight to meet the required WFPS were further dried in an incubator at 40°C (see Supplementary Information, S3, for more information). Once all the cores had attained the target WFPS, they were installed randomly in the system (Fig. 1). The inside edges of the top of the soil cores (ca. 2-4 mm) were carefully sealed with silicone grease to ensure no edge related diffusion effects. This was also done on the bottom of the soil cores, where drying had caused cores to slightly (<1 mm) shrink away from the metal core ring. A circular nylon mesh was placed in the lid groove before installing the cores to prevent soil from falling into the large headspace. The cores were then

lightly tapped into the steel lids of the large headspaces of the incubation vessels with a mallet. The inside walls of the small headspace chambers and where they met the large headspace lids were also greased with silicone to ensure an airtight fit. This was confirmed by measuring gas flow through all 12 cores using a bubble flow meter.

2.4 Soil core incubation

Soil cores were incubated in the dark and the temperature in the laboratory was kept constant at 22°C for the 4-5 day incubation (depending on soil depth). As an acclimatisation period, the soil cores were put into 'flush mode' at a flow rate of 5 ml min^{-1} $core^{-1}$ for *ca.* 18 h with an SF_6-containing (see *2.2*) O_2:N_2 mixture. This mix was 20.9:100 and 13:100 O_2:N_2 for the 0-10 and 50-60 cm cores, respectively. The O_2 content of the mix was chosen by a fitted trend of a similar soil profile (Fig. S3). The acclimatisation period was to allow air-filled pore space to attain the air mix representative of the soil core depths and for the accumulation of a reservoir of SF_6 tracer gas in the headspace below the soil core.

After the 'flush mode', the gas flow was momentarily stopped and the (high SF_6) O_2 cylinder was exchanged for a (ambient-SF_6) compressed air cylinder and the flow adjusted to maintain the same O_2:N_2 ratio. The flow was changed to 'flow over mode' by switching the valve below the large headspace to divert the gas to flow over the small headspace (Fig. 1) and resumed at the same rate (ca. 5 ml min^{-1} $vessel^{-1}$) for the rest of the experiment. The vessels were left for *ca*. 4 h to remove the high SF_6 gas concentrations in the above core headspace from the 'flush mode'. 60 ml of 30 atom% containing 85 and 100 ppm ^{15}N-isotopically labelled N_2O was then syringe-injected into the 0-10 cm and 50-60 cm core large headspace vessels (below the intact soil cores) via the septum (Fig. 1), achieving a $^{15}N_2O$ headspace concentration below the soil core of 2.4 and 2.8 ppm, respectively. These

represent the *in situ* concentrations of N_2O at the same field site between the two depths (ca. 30 cm; Fig. S4). The flow rate was tested daily 3 times per core after sampling using a bubble meter and these specific flow rates were used to calculate fluxes.

2.5 Gas sampling and analysis

Approximately 30 mins after injection of the $^{15}N_2O$ into the headspace below the intact soil cores, the large headspace was assumed to be mixed and the initial '*t* = 0' SF_6 (10 ml) and mass spectrometry (duplicate 12 ml) samples were taken using separate gas-tight 20 ml polypropylene syringes. Samples were assumed to be representative of the large headspace by filling and emptying the syringe 3 times into the headspace before a gas sample was taken. SF_6 samples were analysed immediately, while the duplicate samples for mass spectrometry were injected directly into 12 ml pre-evacuated (flushed with Helium and doubly evacuated) Exetainers® (Labco Ltd., Lampeter, UK). Below core headspace samples were taken daily for SF_6 analysis. Samples from the headspace below the soil core for mass spectrometry were taken at the start (day 1) and end of the incubation (day 3 or 4) so as to limit the removal of gas from the below core headspace. In addition, due to the ability to account for the gas pool from above the core headspace and the SF_6 diffusion, high temporal resolution was not required for the pool dilution calculations. A total of 4% of the volume of gas in the headspace below the soil core was removed for analysis across the incubation period and this was factored in the calculations of the gas concentrations. Headspace above the core were sampled (via the sampling tube) for SF_6 and mass spectrometry (duplicate) analysis daily, with these always taken before headspace below the soil core samples. This was done by disconnecting the sampling tube (see Fig. 1) from the headspace (to avoid creating negative pressure in the system and turbulent mixing with ambient air) and then

connecting a syringe to the tube and taking samples before re-connecting the sampling tube. The volume of the sampling tube (53.4 ml) was sufficient to take 2 samples (maximum of 24 ml) without diluting with ambient air, as was tested (Supplementary Information; S2, Fig. S2).

One of the two duplicate samples was analysed by analysed for N_2O and N_2 concentration and enrichment using a Sercon trace gas analyser and Sercon 20:22 isotope ratio mass spectrometer (Sercon Ltd., Crewe, UK), while the other was spare in case of analysis failure. Samples were stored for 8 months before analysis due to COVID-19 related restrictions to laboratory access and delays. At the same time 12 ml N_2O standards (5 ppm; *n* = 15) were stored with the samples to track any losses of concentration across the storage period. After this period, the mean standard concentration of this stored 5ppm standard was 4.34 ppm ± 0.07. The analysed concentrations were adjusted to compensate for losses during storage.

For the analysis of SF_6, the 10 ml samples were used to flush and fill a 1 ml loop that was then injected directly into a Shimadzu GC-8A (Shimadzu KK, Kyoto, Japan) equipped with an Electron Capture Detector (ECD) and adapted for the rapid and precise analysis of SF_6 in either the gas or water phase (Law et al., 1994). Separation of SF_6 from O_2 and N_2O was achieved by a 3 m by 1/8 ” stainless steel column packed with molecular sieve 5A. The system was calibrated daily using a six-point calibration curve to cover the large range of concentrations observed between the two gas reservoirs. Analytical precision was typically better than 1% and the detection limit was close to 2 pptv.

2.6 Diffusion coefficient (D_s) calculation

The natural logs of SF_6 concentration depletion in the vessels were plotted against

time for each WFPS treatment and soil depth. The diffusion coefficient (D_s) was then calculated from the gradient of the depletion curve using Equation 3.

$$C = \frac{2h \exp(-D_s a_1^2 t/\varepsilon)}{L(a_1^2 + h^2) + h} \quad (3)$$

Where, C is the concentration of gas in the chamber (g m^{-3}); ε is total air-filled porosity (m^3 of air m^{-3} soil); L is the depth of the soil core (m); t is time (h); $h = \varepsilon(a\varepsilon_c)$, where $\varepsilon_c = 1$, is the air content of the chamber (m^3 of air m^{-3} chamber); a is the volume of the chamber per area of soil (m^3 of air m^{-2} soil). A plot of lnC against time becomes linear with slope $-D_s a_1^2 t/\varepsilon$ for sufficiently large t. The value of a_1 can be found using the table in Rolston and Moldrup (2002). The relative diffusion (D_s/D_0) of gas was calculated using the diffusion rate of SF_6 in air, D_0, (0.093 m^2 s^{-1}; Rudolph et al., 1996).

2.7 ^{15}N-N_2O pool dilution calculation

The calculation of gross production and consumption of N_2O was done using the modified (Wen et al., 2017, 2016) ^{15}N-N_2O pool dilution method developed by Yang et al. (2011) from von Fischer and Hedin (2002):

$$[^{14}N_2O]_t = \frac{F_{14} \cdot P}{k_{14} + k_l} - \left(\frac{F_{14} \cdot P}{k_{14} + k_l} - [^{14}N_2O]_0\right) \cdot e\left(-(k_{14} + k_l) \cdot (t - t_0)\right) \quad (4)$$

$$[^{15}N_2O]_t = \frac{F_{15} \cdot P}{k_{15} + k_l} - \left(\frac{F_{15} \cdot P}{k_{15} + k_l} - [^{15}N_2O]_0\right) \cdot e\left(-(k_{15} + k_l) \cdot (t - t_0)\right) \quad (5)$$

Where the concentration of $^{14}N_2O$ at time t ($[^{14}N_2O]_t$) is calculated as the product of the N_2O concentration (ppb) and the ^{14}N-N_2O atom% (i.e. 100 - ^{15}N-N_2O atom%); $[^{15}N_2O]_t$ is the concentration of $^{15}N_2O$ at time t, calculated as the product of the N_2O concentration (ppb) and the ^{15}N-N_2O atom% excess (assuming a ^{15}N isotope composition of background N_2O of 0.3688 atom%; Yang et al., 2011); F_{14} and F_{15} are the $^{14}N_2O$ (0.997) and $^{15}N_2O$ (0.003) mole

fractions of emitted N_2O, respectively; k_{14} and k_{15} are the first-order rate constants of $^{14}N_2O$ and $^{15}N_2O$ reduction to N_2, respectively, calculated using Equation 6 and the average literature value (α = 0.9924 ± 0.0036; Yang et al., 2011) for the stable N isotopic fractionation factors defined as $\alpha = k_{15}/k_{14}$; k_I is the first-order exponential decay constant for SF_6 concentrations over time and represents physical loss via diffusion and/or advection (von Fischer and Hedin, 2002), calculated using Equation 6; t is the time (hours) when the headspace was sampled. The gross N_2O emission (ppb h^{-1}), P, was calculated as the sum of Equations 4 and 5 relative to their mole fractions, solved using MATLAB (MathWorks, Version R2022a, USA).

The first-order rate constants for $^{15}N_2O$ (k_{15}) and SF_6 (k_I) were calculated using the following equation:

$$k = -\frac{ln\left(\frac{C_t}{C_0}\right)}{t} \quad (6)$$

Where k is the first-order rate constant; C_t and C_0 are the concentrations (ppb) of the gas at sampling time t (hours) and at $t = 0$, respectively. The rate constant for $^{14}N_2O$, k_{14}, was calculated by solving $\alpha = k_{15}/k_{14}$, as described above.

The net N_2O emission from the flow-through small headspace was calculated as:

$$F = t \cdot f \cdot (C_{out} - C_{in}) \quad (7)$$

Where F is the flux (ppb h^{-1}); t is the time (h) the sample is representative of; f is the flow rate of air through the headspace (l h^{-1}) and C_{out} and C_{in} are the concentrations of N_2O leaving and entering the headspace (ppb). The results from Equation 7 were then averaged and divided by the total incubation time to give a net flux (ppb h^{-1}) per incubation vessel.

The net emission (Equation 7) and gross production (Equation 6 and 7) N_2O rates were then converted to µg N kg^{-1} h^{-1} using Equation 8.

$$F_E = \frac{F \cdot V_h}{10^{12}} \cdot \frac{p}{R \cdot (T + 273)} \cdot \frac{28}{W_d} \cdot 10^9 \quad (8)$$

Where F_E is either the net emission or gross production of N_2O (µg N kg^{-1} h^{-1}), F is the net or gross emission of N_2O flux in ppb h^{-1}; V_h is the headspace volume (l); R is the ideal gas constant (8.314 J K^{-1} mol^{-1}); p is the pressure (Pa); T is the incubation temperature (°C) and 273 is the conversion constant to Kelvin; 28 is the molecular weight of N in N_2O (g mol^{-1}); W_d is the dry weight of the soil cores (g); 10^{12} and 10^9 are unit conversion factors. Gross N_2O consumption was then calculated as the difference between the gross N_2O production and net N_2O emission (Yang et al., 2011).

2.8 Statistical analysis

All data analysis was done using R (R Core Team, 2017), with figures made using the R package 'ggplot2'(Wickham, 2016). Data were assessed for test assumptions by using the Shapiro-Wilk test ($p > 0.05$) for normality, and Levene's test for homoscedasticity ($p < 0.05$) as well as assessing the qqplots and the residual versus fitted plots. The difference in mean small headspace versus mean large headspace SF_6 fluxes was tested with a Welch Two Sample t-test. Differences in relative diffusivity were tested individually by depth and WFPS with a Welch Two Sample t-test. Difference in fluxes with depth and WFPS were tested by 2-way ANOVAs. Data that did not meet assumptions were log or square root transformed to pass the Shapiro-Wilk and Levene's tests.

3. Results

3.1 Relative diffusivity

As a test to ensure the SF_6 flux results from the small headspace and the depletion of SF_6 from the large headspace corresponded with each other, the fluxes were plotted against each other (Fig. 2). The proximity of the data to the x = y line demonstrate that they

correspond well with each other. This is confirmed by a lack of statistical difference between the fluxes from the small and large headspaces (p = 0.62). The linear trendline (y = 1.26x – 0.29) explained most of the variation in the data (R^2 = 0.96) but its deviation from the x = y line highlights that the mean measured headspace below the soil core flux was overall 16.3% lower than that measured in the headspace above the soil core. While the cores at 70% WFPS (R^2 = 0.55; y = 0.92x + 0.46) more closely aligned with the x=y 1:1 line, substantially more variation was explained by the line for the 50% WFPS cores (R^2 = 0.98; y = 1.21x + 0.54).

The differences in relative diffusivity (D_s/D_0) in the top- and subsoil cores at 50% and 70% WFPS can be seen in Figure 3. In the 0-10 cm depth cores, the diffusivity was significantly lower (79% lower; p <0.001) at 70% WFPS than when incubated at 50% WFPS. A similar trend was found for the 50-60 cm depth soil cores, where the diffusivity was significantly lower (81% lower; p <0.001) at 70% WFPS than when incubated at 50% WFPS. Thus, the overall effect of WFPS on gas diffusivity was significant (p <0.001), while depth the core was taken from was not . While the 50-60 cm cores did have 12% and 21% lower relative diffusivities compared to the 0-10 cm cores at 50% and 70% WFPS, respectively, these differences were not significant (p = 0.54).

3.2 Gross N_2O emission and uptake

The 0-10 cm depth soil cores produced 186% more gross N_2O at 50% WFPS (1.03 $\pm$ 0.46 μg N kg^{-1} ha^{-1}) than at 70% WFPS (0.36 $\pm$ 0.12 μg N kg^{-1} ha^{-1}). Similarly, the 50-60 cm depth cores produced 69% more gross N_2O at 50% WFPS (0.59 $\pm$ 0.04 μg N kg^{-1} ha^{-1}) than at 70% WFPS (0.35 $\pm$ 0.04 μg N kg^{-1} ha^{-1}). As such, the overall effect of WFPS on gross N_2O production was significant (p = 0. 028; Fig. 4a). However, the overall effect of soil depth on gross N_2O production was not significant (p = 0.70), despite the 0-10 cm depth cores (0.69 $\pm$

0.29 μg N kg^{-1} ha^{-1}) producing 47% more gross N_2O than the 50-60 cm cores (0.47 ± 0.04 μg N kg^{-1} ha^{-1}), overall. This was driven by differences between the 50% WFPS cores for the different depths, as there was only a 2% difference in gross N_2O production between the depths at 70% WFPS. For gross N_2O uptake, 216% more N_2O was taken up in the soil at 50% (0.98 ± 0.46 μg N kg^{-1} ha^{-1}) WFPS than at 70% WFPS (0.31 ± 0.12 μg N kg^{-1} ha^{-1}) in the 0-10 cm soil cores. Following a similar trend in the 50-60 cm cores, 69% more N_2O was taken up in the soil at 50% WFPS (0.54 ± 0.03 μg N kg^{-1} ha^{-1}) than at 70% WFPS (0.32 ± 0.04 μg N kg^{-1} ha^{-1}). The overall effect of WFPS on gross N_2O uptake was significant (p = 0.036; Fig. 4b). There was only a 4% difference in gross N_2O uptake between the depths at 70% WFPS, whereas 49% more N_2O was taken up by the 0-10 cm soil cores (0.64 ± 0.29 μg N kg^{-1} ha^{-1}) compared to the 50-60 cm cores (0.43 ± 0.04 μg N kg^{-1} ha^{-1}) at 50% WFPS. Despite this, there was no overall effect of soil depth on gross N_2O uptake (p = 0.97).

3.3 Net N_2O emission

Net emissions of N_2O were overall higher in the cores at 50% WFPS (0.05 ± 0.01 μg N kg^{-1} ha^{-1}) than at 70% (0.04 ± 0.001 μg N kg^{-1} ha^{-1}, p = 0.042). This difference was driven by the 41% lower emissions from the 70% cores at 50-60 cm (0.03 ± 0.002 μg N kg^{-1} ha^{-1}; Fig. 4c) compared to the 0-10 cm cores at the same WFPS (0.05 ± 0.01 μg N kg^{-1} ha^{-1}). In the 50-60 cm cores, the emissions from the 50% WFPS (0.04 ± 0.002 μg N kg^{-1} ha^{-1}) treatment were 52% higher than in the 70% WFPS (0.03 ± 0.002 μg N kg^{-1} ha^{-1}) treatment, but 5% lower than from the 70% WFPS cores. Overall, the 0-10 cm soil cores had 30% higher net N_2O emissions (0.05 ± 0.01 μg N kg^{-1} h^{-1}) compared to the deeper soil cores (0.04 ± 0.002 μg N kg^{-1} h^{-1}; p = 0.014; Fig. 4c).

4. Discussion

4.1 Soil diffusivity

While the agreement between the small and large headspace SF_6 fluxes was good (Fig. 2), we attribute the overall higher fluxes in the headspace above the core compared to the headspace below the core is likely due to a technical factors. Due to the sampling of the headspaces above the cores prior to those below (to avoid any negative pressure influencing the above core headspace sample), there was a 1-2 h time delay between these as the samples needed to be injected directly into the GC. Considering the exponential depletion of SF_6 from the headspace below the cores, this time lag would translate to slightly different fluxes. Therefore, we believe the difference between the calculated fluxes is predominantly due to the delay in above core headspace samples. We believe the nature of the fit to be within an acceptable range of error for the relationship between the small and large headspaces to produce meaningful results from the ^{15}N-N_2O pool dilution.

The relative diffusivity values in Figure 2 (0.024 – 0.480) are consistent with the expected values for the exponential increase in D_s/D_0 with increasing air-filled pore porosity for soils with different overall pore architectures (Hashimoto and Komatsu, 2006) and using different measuring techniques (Allaire et al., 2008). The hypothesis that soil diffusion would be reduced by both increasing depth and WFPS was only partly confirmed (Fig. 3). As expected, the highest WFPS in the soil reduced gas diffusivity of the soil substantially, but the different inherent physical soil characteristics (bulk density, porosity, texture; Table 1) of the cores did not affect the D_s/D_0 of the soil when at the same WFPS. Fujikawa and Miyazaki (2005) found D_s/D_0 to increase with higher bulk density which they attributed to lower total porosity via the change in shape and size of pores which can be assumed to restrict gas movement, consistent with other studies (Balaine et al., 2013; Currie, 1984). However, these

studies were all done on sieved and repacked soil which would create a more homogenous soil pore structure and can cause significant errors in determining the 'true' D_s/D_0 (Allaire et al., 2008). The inherent pore structure and preferential flow pathways (i.e. macropores, soil pipes and cracks) were preserved in the cores (though edge related diffusion was avoided by sealing these) and this heterogeneity is a primary factor driving gas flow and is very important for studying gas diffusion (Allaire et al., 2008; Chamindu Deepagoda et al., 2019; Guo and Lin, 2018). However, no difference in D_s/D_0 between intact soil cores at a range of depths, bulk densities and porosities have also been observed (Chamindu Deepagoda et al., 2019). We attribute this lack of difference between depths to the presence of natural macropores, pipes and preferential flow paths that create similarities in the diffusivity of gas through the soil and the differences in soil physical properties was not sufficient to drive differences in D_s/D_0.

4.2 Gross N_2O uptake

Evidence for N_2O consumption by soils is extensive in the literature (see review by Chapuis-Lardy et al., 2007). In our study, we report gross N_2O-N uptake rates ranging from 0.03 – 2.79 µg N kg^{-1} h^{-1} (Fig. 4b) which is a similar range to that measured by others in similar agricultural soils (Clough et al., 2006; Luo et al., 2022; Wen et al., 2016). N_2O consumption rates, in our study, correlated closely with production rates, which is consistent with other studies (Wen et al., 2016; Yang et al., 2011; Yang and Silver, 2016), suggesting that consumption increased proportionally with N_2O production (Fig. 4a, b). These results uncovered a high potential for N_2O uptake that would have been masked by higher N_2O production had only the latter been measured.

The hypothesis that the uptake of N_2O would be greater in the more microbially-active topsoil compared to the subsoil was rejected (Fig. 4b). While the uptake rate was highest in the topsoil cores at 50% WFPS, there was no statistical difference between depths. This is

despite there being a lower microbial biomass (indicating size of the microbial community; Table 1) and a lower abundance of denitrification (*nirK*, *nirS*) and complete denitrification (*nosZ*) gene copies in the subsoil (indicating denitrification potential of the microbial community; Table S1). Scaling the magnitude of N_2O uptake relative to the size and denitrification potential of the soil microbial community, it was much greater in the subsoil compared to the topsoil. Care should be taken with this interpretation as microbial biomass size does not necessarily indicate the activity of denitrifiers, and gene abundance does not necessarily link to process rates as discussed in a meta-analysis conducted by Rocca et al. (2015).

The reduction of N_2O to N_2 can be considerable in the subsoil, dependent on a combination of inherent soil characteristics (C, NO_3^-) and physical conditions (WFPS, O_2 concentration, diffusivity) (Clough et al., 2005, 1999; Semedo et al., 2020). Within the topsoil the organic C, total N, dissolved organic C, dissolved organic N and extractable NO_3^- were greater than that found in the subsoil (Table 1). Thus, labile C and N substrate supply likely differed between depths during the course of the experiment. As discussed previously, NO_3^- can outcompete N_2O as the terminal electron acceptor during complete denitrification (Chapuis-Lardy et al., 2007), potentially contributing to differences in N_2O uptake rates between depths. Additionally, the cores in this study were incubated at an O_2 content similar to their *in situ* levels - which was 20.9% and 13% in the topsoil and subsoil incubations. Due to 38% less O_2 in the subsoil cores, the formation of semi-anaerobic and full anaerobic conditions required for N_2O production and consumption would be more easily achieved. This is supported by others that found increased denitrification when O_2 was restricted (Patureau et al., 1996; Schlüter et al., 2018), which would explain the lack of difference in gross N_2O uptake between soil depths.

Higher WFPS decreases the diffusion of N_2O produced in the soil to the surface and increases its residence time allowing for higher potential of complete denitrification of N_2O to N_2 (Balaine et al., 2013; Chamindu Deepagoda et al., 2019). While the diffusion rate did decrease with greater WFPS (Fig. 3), this did not produce a difference between the N_2O uptake rates of the soil cores incubated at different WFPS levels. In fact, the 50% WFPS cores had higher consumption rates. We therefore reject our final hypothesis, that N_2O uptake would be higher with increasing WFPS.

N_2O consumption is generally expected to occur under conditions of low N availability and high soil moisture (Chapuis-Lardy et al., 2007). While there is extensive literature that suggests there is a high WFPS 'critical threshold' at which consumption predominantly takes place (ca. >60-80%; Bateman and Baggs, 2005; Chamindu Deepagoda et al., 2019; Davidson, 1991), there are studies that have found no differences or even an increase in N_2O uptake with lower WFPS (Goldberg and Gebauer, 2009; Khalil et al., 2002; Rosenkranz et al., 2006; Wu et al., 2013) and low N (Wang et al., 2018). A possible explanation for N_2O consumption in drier soil is greater diffusivity allowing N_2O present in air or headspace to diffuse to the denitrification site, where in the absence of NO_3^-, N_2O may be used as an electron acceptor for denitrification (Chapuis-Lardy et al., 2007). Bazylinski et al. (1986) demonstrated this in isolated denitrifier growth using only N_2O as an electron acceptor. Though, due to the presence of NO_3^- in the top- and subsoil (Table 1) this is unlikely to contribute substantially. A possible alternative pathway is aerobic nitrate reduction, which is the bacterial reduction of NO_3^- in aerobic conditions that can occur independently of denitrification gas-producing reactions and is an underappreciated nitrate sink according to Roco et al. (2016). However, despite 84% more NO_3^- in the topsoil compared to the subsoil (Table 1), no significant difference was measured between cores from these depths suggesting that this may not have

been the primary mechanism. Without information on the changes in N pools it is not possible to determine the occurrence of this process. However, it suggests that substantial N_2O consumption in our study could be driven directly and/or indirectly by aerobic processes rather than anaerobic denitrification processes (Wang et al., 2018; Wu et al., 2013). If this is the case and anaerobic microsites were not an important location for denitrification in this study, the calculated gross N_2O production and consumption fluxes may be more accurate than expected from the pool dilution results. This is because the ^{15}N-N_2O pool dilution method does not allow for accurate measurement of gross production and consumption of N_2O in situations most likely to be occurring within anaerobic microsites. These are when i) N_2O produced is immediately consumed within the cells of denitrifiers, and ii) produced N_2O diffuses out of denitrifiers and is taken up by other microbes without mixing with the $^{15}N_2O$ label during the measurement period (Wen et al., 2016). Due to the 58% smaller volumes of the cores in this study compared to Wen et al. (2016), these processes may have been less likely to occur due to shorter diffusion distances reducing the time N_2O spent in the soil and therefore the potential for its consumption in microsites.

4.3 Gross N_2O emission

Gross N_2O emission rates varied from 0.056 to 2.83 μg N kg^{-1} h^{-1} (Fig. 4a), which is within the range of measurements reported in other studies (Clough et al., 2006; Luo et al., 2022; Wen et al., 2016). These rates may be low as N_2O can be lost rapidly (hours) after wetting (Barrat et al., 2022; Smith and Tiedje, 1979). As the cores were brought to the desired WFPS ca. 18 h before the incubation, they may have already lost substantial soil N prior to incubation.

N_2O production is driven by microbial denitrification and nitrification in the soil under partially anaerobic and aerobic conditions (Chapuis-Lardy et al., 2007; Diba et al., 2011). The

dominating process has been found to change from nitrification to denitrification at WFPS of 60-70% (Bateman and Baggs, 2005; Pihlatie et al., 2004). This would suggest that the N_2O produced in the 50% and 70% WFPS cores was predominantly from nitrification or denitrification, respectively. However, these may occur in the soil simultaneously (Bateman and Baggs, 2005; Pihlatie et al., 2004). Denitrification is a common source of N_2O in many agricultural soils, and the close coupling between gross emission and uptake of N_2O as found in this study (Fig. 4a, b), suggests denitrification was the dominant process (Chapuis-Lardy et al., 2007; Wen et al., 2016). According to Davidson (1991), N_2O production is greatest when at or near field capacity (ca. 60% WFPS) as nitrification and denitrification rates are comparable sources of N_2O occurring simultaneously. Therefore, a higher gross N_2O emission in the soil cores at 50% WFPS could be explained by simultaneous denitrification and nitrification producing N_2O. Nevertheless, we lack information to be able to source partition the N_2O generated in this study. Recent advances in N_2O isotopomer measurements are shedding light on microbial source partitioning of N_2O e.g. Stuchiner and von Fischer (2022b) demonstrate denitrification was the predominant N_2O production pathway in soils ranging from 50-95% WFPS and Harris et al. (2021) found that he proportion of N_2O from denitrification did not decrease under even very low WFPS.

Gross emission rates were not different with depth in this study (Fig. 4a). Emission rates of N_2O have been observed to be higher in subsoil than in topsoil under certain conditions (Goldberg et al., 2008; Müller et al., 2004; Shcherbak and Robertson, 2019). This may be due to denser, deeper soils becoming anaerobic more quickly as a result of a restriction in diffusivity and lower pore volume (Berisso et al., 2013). As the subsoil cores were incubated with almost 38% less O_2 than the topsoil, the formation of semi-anaerobic and full anaerobic conditions required for N_2O production would be more easily achieved. Therefore,

despite higher biological N_2O production potential in the topsoil (Table 1), it would suggest that physical N_2O-promoting conditions in the subsoil can match this potential.

4.4 Net N_2O emission

Net emissions from the soil cores varied between 0.025-0.084 μg N kg^{-1} h^{-1} (Fig. 4c). This low emission rate is expected from an unfertilized, low N arable soil (Table 1; Wen et al., 2016). The net N_2O emission decreased with soil depth which is primarily due to the low rate from the 70% WFPS 50-60 cm cores (Fig. 4c). This trend reflects the gross N_2O uptake and emission in the soil, as the net emission is the gross consumption subtracted from the gross emission.

5. Conclusions

Using a novel dual-headspace system for soil core incubation, we demonstrated that this method is reliable for measuring fluxes both above and below a soil core at controlled O_2 concentration and for applying the ^{15}N-N_2O pool dilution method. The fluxes measured from this system all fall within previously measured ranges measured in the field. We believe using a headspace both above and below the soil core is better than a single headspace approach as it is better placed to replicate the movement of gas through the soil and better mix gas from the reservoir with soil air. Though this will require comparative testing. We provide evidence that the relative diffusivity of gas within intact soil cores does not differ with soil depth, likely due to the preservation of preferential flow pathways. This contrasts with studies that use sieved and repacked cores which allow for more equal mixing of labelled and non-labelled isotope pools, but do not represent or measure true soil diffusivity. Gross N_2O production and consumption rates did not differ with depth but were higher in the 50% WFPS

cores. We attribute this to aerobic denitrification and simultaneous denitrification and nitrification for N_2O consumption and production, respectively. We contribute further evidence challenging the hypothesis that only wet soils play a crucial role in N_2O production, consumption and net emissions. In addition, we challenge the notion that only soils with net negative emissions experience substantial N_2O consumption rates. The results from this study provide a novel application of the ^{15}N-N_2O pool dilution method and important evidence of N_2O production and consumption fluxes in low-N status, arable soil at different depths.

Acknowledgements

This work was supported by the FLEXIS (Flexible Integrated Energy Systems) programme, an operation led by Cardiff University, Swansea University and the University of South Wales and funded through the Welsh European Funding Office (WEFO). Rothamsted Research is supported by the Biotechnology and Biological Sciences Research Council (BBSRC, grants BBS/E/C/000I0310 and BBS/E/C/000I0320). The authors would like to thank Plymouth Marine Laboratory for the loan of the SF_6 GC. Sincere thanks also to Alan Jones for his excellent engineering advice and work; Lucy Greenfield for helping with the fieldwork; Nadine Loick and Neil Donovan for their technical support; Alex Boon for his help with the diffusion calculations and Marife Corre for her help with the pool dilution calculations. We thank the anonymous reviewers for their careful reading of the manuscript and their many insightful comments and suggestions.

ESB, LMC, DRC and DLJ conceived the study. ESB conducted the experiments and wrote the manuscript, with specialist technical support from PDN and ERD. KAM supported ESB with the pool dilution calculations and interpretation. All authors reviewed the manuscript.

References

Allaire, S.E., Lafond, J.A., Cabral, A.R., Lange, S.F., 2008. Measurement of gas diffusion through soils: Comparison of laboratory methods. J. Environ. Monit. 10, 1326–1336. https://doi.org/10.1039/b809461f

Almaraz, M., Wong, M.Y., Yang, W.H., 2020. Looking back to look ahead: a vision for soil denitrification research. Ecology 101, 1–10. https://doi.org/10.1002/ecy.2917

Balaine, N., Clough, T.J., Beare, M.H., Thomas, S.M., Meenken, E.D., Ross, J.G., 2013. Changes in Relative Gas Diffusivity Explain Soil Nitrous Oxide Flux Dynamics. Soil Sci. Soc. Am. J. 77, 1496–1505. https://doi.org/10.2136/sssaj2013.04.0141

Barrat, H.A., Clark, I.M., Evans, J., Chadwick, D.R., Cardenas, L., 2022. The impact of drought length and intensity on N cycling gene abundance, transcription and the size of an N_2O hot moment from a temperate grassland soil. Soil Biol. Biochem. 168, 108606. https://doi.org/10.1016/j.soilbio.2022.108606

Bateman, E.J., Baggs, E.M., 2005. Contributions of nitrification and denitrification to N_2O emissions from soils at different water-filled pore space. Biol. Fertil. Soils 41, 379–388. https://doi.org/10.1007/s00374-005-0858-3

Bazylinski, D.A., Soohoo, C.K., Hollocher, T.C., 1986. Growth of Pseudomonas aeruginosa on nitrous oxide. Appl. Environ. Microbiol. 51, 1239–1246. https://doi.org/10.1128/aem.51.6.1239-1246.1986

Berisso, F.E., Schjønning, P., Keller, T., Lamandé, M., Simojoki, A., Iversen, B. V., Alakukku, L., Forkman, J., 2013. Gas transport and subsoil pore characteristics: Anisotropy and long-term effects of compaction. Geoderma 195–196, 184–191.

https://doi.org/10.1016/j.geoderma.2012.12.002

Blagodatsky, S., Smith, P., 2012. Soil physics meets soil biology: Towards better mechanistic prediction of greenhouse gas emissions from soil. Soil Biol. Biochem. 47, 78–92. https://doi.org/10.1016/j.soilbio.2011.12.015

Boon, A., Robinson, J.S., Nightingale, P.D., Cardenas, L., Chadwick, D.R., Verhoef, A., 2013. Determination of the gas diffusion coefficient of a peat grassland soil. Eur. J. Soil Sci. 64, 681–687. https://doi.org/10.1111/ejss.12056

Boyer, E.W., Alexander, R.B., Parton, W.J., Li, C., Butterbach-Bahl, K., Donner, S.D., Skaggs, R.W., Del Grosso, S.J., 2006. Modeling denitrification in terrestrial and aquatic ecosystems at regional scales. Ecol. Appl. 16, 2123–2142. https://doi.org/10.1890/1051-0761(2006)016[2123:MDITAA]2.0.CO;2

Butterbach-Bahl, K., Baggs, E.M., Dannenmann, M., Kiese, R., Zechmeister-Boltenstern, S., 2013. Nitrous oxide emissions from soils: how well do we understand the processes and their controls? Philos. Trans. R. Soc. B: Biol. Sci. 368, 20130122. https://doi.org/10.1098/rstb.2013.0122

Cárdenas, L.M., Hawkins, J.M.B., Chadwick, D., Scholefield, D., 2003. Biogenic gas emissions from soils measured using a new automated laboratory incubation system. Soil Biol. Biochem. 35, 867–870. https://doi.org/10.1016/S0038-0717(03)00092-0

Chamindu Deepagoda, T.K.K., Jayarathne, J.R.R.N., Clough, T.J., Thomas, S., Elberling, B., 2019. Soil-Gas Diffusivity and Soil-Moisture effects on N_2O Emissions from Intact Pasture Soils . Soil Sci. Soc. Am. J. 83, 1032–1043. https://doi.org/10.2136/sssaj2018.10.0405

Chapuis-Lardy, L., Wrage, N., Metay, A., Chotte, J.L., Bernoux, M., 2007. Soils, a sink for N_2O? A review. Glob. Chang. Biol. 13, 1–17. https://doi.org/10.1111/j.1365-2486.2006.01280.x

Clough, T.J., Jarvis, S.C., Dixon, E.R., Stevens, R.J., Laughlin, R.J., Hatch, D.J., 1999. Carbon induced subsoil denitrification of ^{15}N-labelled nitrate in 1 m deep soil columns. Soil Biol. Biochem. 31, 31–41. https://doi.org/10.1016/S0038-0717(98)00097-2

Clough, T.J., Kelliher, F.M., Wang, Y.P., Sherlock, R.R., 2006. Diffusion of ^{15}N-labelled N_2O into soil columns: a promising method to examine the fate of N_2O in subsoils. Soil Biol. Biochem. 38, 1462–1468. https://doi.org/10.1016/j.soilbio.2005.11.002

Clough, T.J., Sherlock, R.R., Rolston, D.E., 2005. A review of the movement and fate of N_2O in the subsoil. Nutr. Cycl. Agroecosystems 72, 3–11. https://doi.org/10.1007/s10705-004-7349-z

Currie, J.A., 1984. Gas diffusion through soil crumbs: the effects of wetting and swelling. J. Soil Sci. 34, 217–232. https://doi.org/10.1111/j.1365-2389.1983.tb01029.x

Currie, J.A., 1960. Gaseous diffusion in porous media Part 1. - A non-steady state method. Br. J. Appl. Phys. 11, 314–317. https://doi.org/10.1088/0508-3443/11/8/302

Davidson, E.A., 1991. Fluxes of nitrous oxide and nitric oxide from terrestrial ecosystems. Microb. Prod. Consum. Greenh. Gases Methane, Nitrous Oxide, Halomethanes 219–235.

Davidson, E.A., Ishida, F.Y., Nepstad, D.C., 2004. Effects of an experimental drought on soil emissions of carbon dioxide, methane, nitrous oxide, and nitric oxide in a moist tropical forest. Glob. Chang. Biol. 10, 718–730. https://doi.org/10.1111/j.1529-

8817.2003.00762.x

Diba, F., Shimizu, M., Hatano, R., 2011. Effects of soil aggregate size, moisture content and fertilizer management on nitrous oxide production in a volcanic ash soil. Soil Sci. Plant Nutr. 57, 733–747. https://doi.org/10.1080/00380768.2011.604767

Dong, W., Wang, Y., Hu, C., 2013. Concentration profiles of CH_4, CO_2 and N_2O in soils of a wheat–maize rotation ecosystem in North China Plain, measured weekly over a whole year. Agric. Ecosyst. Environ. 1, 260–272. https://doi.org/https://doi.org/10.1016/j.agee.2012.10.004

Fujikawa, T., Miyazaki, T., 2005. Effects of bulk density and soil type on the gas diffusion coefficient in repacked and undisturbed soils. Soil Sci. 170, 892–901. https://doi.org/10.1097/01.ss.0000196771.53574.79

Giles, M.E., Daniell, T.J., Baggs, E.M., 2017. Compound driven differences in N_2 and N_2O emission from soil; the role of substrate use efficiency and the microbial community. Soil Biol. Biochem. 106, 90-98. https://doi.org/10.1016/j.soilbio.2016.11.028

Goldberg, S.D., Gebauer, G., 2009. Drought turns a Central European Norway spruce forest soil from an N_2O source to a transient N_2O sink. Glob. Chang. Biol. 15, 850–860. https://doi.org/10.1111/j.1365-2486.2008.01752.x

Goldberg, S.D., Knorr, K.H., Gebauer, G., 2008. N_2O concentration and isotope signature along profiles provide deeper insight into the fate of N_2O in soils. Isotopes Environ. Health Stud. 44, 377–391. https://doi.org/10.1080/10256010802507433

Groffman, P.M., Altabet, M.A., Böhlke, H., Butterbach-Bahl, K., David, M.B., Firestone, M.K., Giblin, A.E., Kana, T.M., Nielsen, L.P. and Voytek, M.A., 2006. Methods for measuring

denitrification: diverse approaches to a difficult problem. Ecological applications, 16, 2091-2122.

Guo, L., Lin, H., 2018. Addressing Two Bottlenecks to Advance the Understanding of Preferential Flow in Soils, 1st ed, Advances in Agronomy. Elsevier Inc. https://doi.org/10.1016/bs.agron.2017.10.002

Harris, E., Diaz-Pines, E., Stoll, E., Schloter, M., Schulz, S., Duffner, C., Li, K., Moore, K.L., Ingrisch, J., Reinthaler, D., Zechmeister-Boltenstern, S., Glatzel, S., Brüggemann, N., Bahn, M., 2021. Denitrifying pathways dominate nitrous oxide emissions from managed grassland during drought and rewetting. Sci. Adv. 7, eabb7118. https://doi.org/10.1126/sciadv.abb7118

Hashimoto, S., Komatsu, H., 2006. Relationships between soil CO_2 concentration and CO_2 production, temperature, water content, and gas diffusivity: Implications for field studies through sensitivity analyses. J. For. Res. 11, 41–50. https://doi.org/10.1007/s10310-005-0185-4

Hill, A.R., Cardaci, M., 2004. Denitrification and Organic Carbon Availability in Riparian Wetland Soils and Subsurface Sediments. Soil Sci. Soc. Am. J. 68, 320–325. https://doi.org/10.2136/sssaj2004.3200a

Jahangir, M.M.R., Khalil, M.I., Johnston, P., Cardenas, L.M., Hatch, D.J., Butler, M., Barrett, M., O, V., Richards, K.G., 2012. Denitrification potential in subsoils : A mechanism to reduce nitrate leaching to groundwater. Agriculture, Ecosyst. Environ. 147, 13–23. https://doi.org/10.1016/j.agee.2011.04.015

Jia, G., Shevliakova, Elena, Artaxo, Paulo, De Noblet-Ducoudré, Nathalie, Houghton, Richard,

Anderegg, W., Bernier, P., Carlo Espinoza, J., Semenov, S., Xu, X., Shevliakova, E, Artaxo, P, De Noblet-Ducoudré, N, Houghton, R, House, J., Kitajima, K., Lennard, C., Popp, A., Sirin, A., Sukumar, R., Verchot, L., 2019. Land-climate interactions. Clim. Chang. L. an IPCC Spec. Rep. Clim. Chang. Desertif. L. Degrad. Sustain. L. Manag. food Secur. Greenh. gas fluxes Terr. Ecosyst. 131–248.

Khalil, M.I., Rosenani, A.B., Van Cleemput, O., Fauziah, C.I., Shamshuddin, J., 2002. Nitrous Oxide Emissions from an Ultisol of the Humid Tropics under Maize-Groundnut Rotation. J. Environ. Qual. 31, 1071–1078. https://doi.org/10.2134/jeq2002.1071

Laughlin, R.J., Stevens, R.J., 2002. Evidence for Fungal Dominance of Denitrification and Codenitrification in a Grassland Soil. Soil Sci. Soc. Am. J. 66, 1540–1548. https://doi.org/10.2136/sssaj2002.1540

Laughlin, R.J., Stevens, R.J., Zhuo, S., 1997. Determining Nitrogen-15 in Ammonium by Producing Nitrous Oxide. Soil Sci. Soc. Am. J. 61, 462. https://doi.org/10.2136/sssaj1997.03615995006100020013x

Law, C.S., Watson, A.J., Liddicoat, M.I., 1994. Automated vacuum analysis of sulphur hexafluoride in seawater: derivation of the atmospheric trend (1970-1993) and potential as a transient tracer. Mar. Chem. 48, 57–69. https://doi.org/10.1016/0304-4203(94)90062-0

Li, Z., Kelliher, F.M., 2005. Determining nitrous oxide emissions from subsurface measurements in grazed pasture: A field trial of alternative technology. Aust. J. Soil Res. 43, 677–687. https://doi.org/10.1071/SR04106

Liu, R., Hu, H., Suter, H., Hayden, H.L., He, J., Mele, P., Chen, D., 2016. Nitrification is a

primary driver of nitrous oxide production in laboratory microcosms from different land-use soils. Front. Microbiol. 7, 1373. doi: 10.3389/fmicb.2016.01373

Luo, J., Beule, L., Shao, G., Veldkamp, E., Corre, M.D., 2022. Reduced Soil Gross N_2O Emission Driven by Substrates Rather Than Denitrification Gene Abundance in Cropland Agroforestry and Monoculture. J. Geophys. Res. Biogeosciences 127, 1–16. https://doi.org/10.1029/2021jg006629

Müller, C., Stevens, R.J., Laughlin, R.J., Jäger, H.J., 2004. Microbial processes and the site of N2O production in a temperate grassland soil. Soil Biol. Biochem. 36, 453–461. https://doi.org/10.1016/j.soilbio.2003.08.027

Neftel, A., Flechard, C., Ammann, C., Conen, F., Emmenegger, L., Zeyer, K., 2007. Experimental assessment of N_2O background fluxes in grassland systems. Tellus, Ser. B Chem. Phys. Meteorol. 59, 470–482. https://doi.org/10.1111/j.1600-0889.2007.00273.x

Patureau, D., Bernet, N., Moletta, R., 1996. Effect of oxygen on denitrification in continuous chemostat culture with Comamonas sp SGLY2. J. Ind. Microbiol. Biotechnol. 16, 124–128. https://doi.org/10.1007/bf01570072

Pihlatie, M., Syväsalo, E., Simojoki, A., Esala, M., Regina, K., 2004. Contribution of nitrification and denitrification to N_2O production in peat, clay and loamy sand soils under different soil moisture conditions. Nutr. Cycl. Agroecosystems 70, 135–141. https://doi.org/10.1023/B:FRES.0000048475.81211.3c

R Core Team, 2017. A language and environment for statistical computing. R.

Richardson, D., Felgate, H., Watmough, N., Thomson, A., Baggs, E., 2009. Mitigating release

of thepotent greenhouse gas N2O from the nitrogen cycle - could enzymic regulation hold the key? Trends Biotechnol. 27, 388-397. https://doi.org/10.1016/j.tibtech.2009.03.009

Rocca, J.D., Hall, E.K., Lennon, J.T., Evans, S.E., Waldrop, M.P., Cotner, J.B., Nemergut, D.R., Graham, E.B., Wallenstein, M.D., 2015. Relationships between protein-encoding gene abundance and corresponding process are commonly assumed yet rarely observed. ISME J. 9, 1693-1699. 10.1038/ismej.2014.252

Roco, C.A., Bergaust, L.L., Shapleigh, J.P., Yavitt, J.B., 2016. Reduction of nitrate to nitrite by microbes under oxic conditions. Soil Biol. Biochem. 100, 1–8. https://doi.org/10.1016/j.soilbio.2016.05.008

Rolston, D.E., Moldrup, P., 2002. 4.3 Gas Diffusivity, in: Methods of Soil Analysis: Part 4 Physical Methods. pp. 1113–1139.

Rosenkranz, P., Bruggemann, N., Papen, H., Xu, Z., Seufert, G., Butterbach-Bahl, K., 2006. N_2O, NO and CH_4 exchange, and microbial N turnover over a Mediterranean pine forest soil. Environ. Res. 121–133.

Rudolph, J., Rothfuss, F., Conrad, R., 1996. Flux between soil and atmosphere, vertical concentration profiles in soil, and turnover of nitric oxide: 1. Measurements on a model soil core. J. Atmos. Chem. 23, 253–273. https://doi.org/10.1007/BF00055156

Schlesinger, W.H., 2013. An estimate of the global sink for nitrous oxide in soils. Glob. Chang. Biol. 19, 2929–2931. https://doi.org/10.1111/gcb.12239

Schlüter, S., Henjes, S., Zawallich, J., Bergaust, L., Horn, M., Ippisch, O., Vogel, H.J., Dörsch, P., 2018. Denitrification in soil aggregate analogues-effect of aggregate size and oxygen

diffusion. Front. Environ. Sci. 6, 1–10. https://doi.org/10.3389/fenvs.2018.00017

Semedo, M., Wittorf, L., Hallin, S., Song, B., 2020. Differential expression of clade i and II N_2O reductase genes in denitrifying Thauera linaloolentis 47LolT under different nitrogen conditions. FEMS Microbiol. Lett. 367, 1–6. https://doi.org/10.1093/femsle/fnaa205

Sexstone, A.J., Revsbech, N.P., Parkin, T.B., Tiedje, J.M., 1985. Direct Measurement of Oxygen Profiles and Denitrification Rates in Soil Aggregates. Soil Sci. Soc. Am. J. 49, 645–651. https://doi.org/10.2136/sssaj1985.03615995004900030024x

Shcherbak, I., Robertson, G.P., 2019. Nitrous Oxide (N_2O) Emissions from Subsurface Soils of Agricultural Ecosystems. Ecosystems 22, 1650–1663. https://doi.org/10.1007/s10021-019-00363-z

Smith, M.S., Tiedje, J.M., 1979. Phases of denitrification following oxygen depletion in soil. Soil Biol. Biochem. 11, 261–267. https://doi.org/10.1016/0038-0717(79)90071-3

Stuchiner, E.R., von Fischer, J.C., 2022a. Using isotope pool dilution to understand how organic carbon additions affect N_2O consumption in diverse soils . Glob. Chang. Biol. 0–2. https://doi.org/10.1111/gcb.16190

Stuchiner, E.R., von FIscher, J.C., 2022b. Characterizing the importance of denitrification for N2O production in soils using natural abundance and isotopic labeling techniques. J. Geophys. Res. Biogeosci. 127, e2021JG006555. https://doi.org/10.1029/2021JG006555

Van Beek, C.L., Hummelink, E.W.J., Velthof, G.L., Oenema, O., 2004. Denitrification rates in relation to groundwater level in a peat soil under grassland. Biol. Fertil. Soils 39, 329–336. https://doi.org/10.1007/s00374-003-0685-3

van Bochove, E., Bertrand, N., Caron, J., 1998. In Situ Estimation of the Gaseous Nitrous Oxide Diffusion Coefficient in a Sandy Loam Soil. Soil Sci. Soc. Am. J. 62, 1178–1184. https://doi.org/10.2136/sssaj1998.03615995006200050004x

Van Cleemput, O., 1998. Subsoils: Chemo- and biological denitrification, N_2O and N_2 emissions. Nutr. Cycl. Agroecosystems 52, 187–194. https://doi.org/10.1023/a:1009728125678

Van Groenigen, J.W., Zwart, K.B., Harris, D., Van Kessel, C., 2005. Vertical gradients of $\delta^{15}N$ and $\delta^{18}O$ in soil atmospheric N_2O - Temporal dynamics in a sandy soil. Rapid Commun. Mass Spectrom. 19, 1289–1295. https://doi.org/10.1002/rcm.1929

von Fischer, J.C., Hedin, L.O., 2002. Separating methane production and consumption with a field-based isotope pool dilution technique. Global Biogeochem. Cycles 16, 8-1-8–13. https://doi.org/10.1029/2001gb001448

Wang, Y., Li, X., Dong, W., Wu, D., Hu, C., Zhang, Y., Luo, Y., 2018. Depth-dependent greenhouse gas production and consumption in an upland cropping system in northern China. Geoderma 319, 100–112. https://doi.org/10.1016/j.geoderma.2018.01.001

Wen, Y., Chen, Z., Dannenmann, M., Carminati, A., Willibald, G., Kiese, R., Wolf, B., Veldkamp, E., Butterbach-Bahl, K., Corre, M.D., 2016. Disentangling gross N_2O production and consumption in soil. Sci. Rep. 6, 1–8. https://doi.org/10.1038/srep36517

Wen, Y., Corre, M.D., Schrell, W., Veldkamp, E., 2017. Gross N_2O emission and gross N_2O uptake in soils under temperate spruce and beech forests. Soil Biol. Biochem. 112, 228–236. https://doi.org/10.1016/j.soilbio.2017.05.011

Wickham, H., 2016. Elegant Graphics for Data Analysis. ggplot2.

WRB, 2014. World Reference Base (WRB) for Soil Resources (updated 2015). International soil classification system for naming soils and creating legends for soil maps. World Soil Resources Reports No. 106. FAO, Rome.

Wu, D., Dong, W., Oenema, O., Wang, Y., Trebs, I., Hu, C., 2013. N_2O consumption by low-nitrogen soil and its regulation by water and oxygen. Soil Biol. Biochem. 60, 165–172. https://doi.org/10.1016/j.soilbio.2013.01.028

Yang, W.H., Silver, W.L., 2016. Net soil-atmosphere fluxes mask patterns in gross production and consumption of nitrous oxide and methane in a managed ecosystem. Biogeosciences 13, 1705–1715. https://doi.org/10.5194/bg-13-1705-2016

Yang, W.H., Teh, Y.A., Silver, W.L., 2011. A test of a field-based ^{15}N-nitrous oxide pool dilution technique to measure gross N_2O production in soil. Glob. Chang. Biol. 17, 3577–3588. https://doi.org/10.1111/j.1365-2486.2011.02481.x

Zhang, Y., Mu, Y., Zhou, Y., Tian, D., Liu, J., Zhang, C., 2016. NO and N_2O emissions from agricultural fields in the North China Plain: Origination and mitigation. Sci. Total Environ. 551–552, 197–204. https://doi.org/10.1016/j.scitotenv.2016.01.209

Zona, D., Janssens, I.A., Gioli, B., Jungkunst, H.F., Serrano, M.C., Ceulemans, R., 2013. N_2O fluxes of a bio-energy poplar plantation during a two years rotation period. GCB Bioenergy 5, 536–547. https://doi.org/10.1111/gcbb.12019

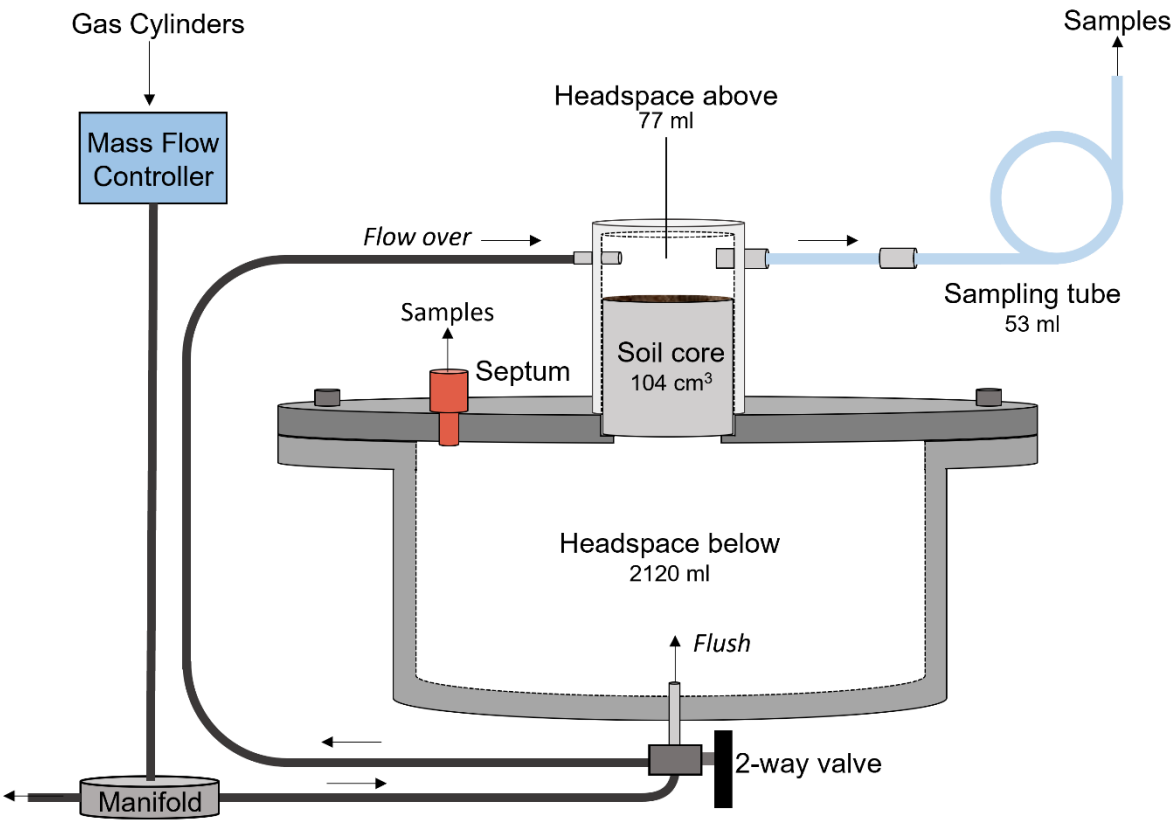

Fig. 1 The dual-headspace system used for incubating the soil cores in this study. The system can be placed in 2 different modes, 'flush' and 'flow over'. The former is where air flow from the gas cylinders is directed to enter via the headspace below the core, while the latter directs this air via the headspace above the soil core. All dimensions, materials and a photograph of the system can be found in the Supplementary Information (S1).

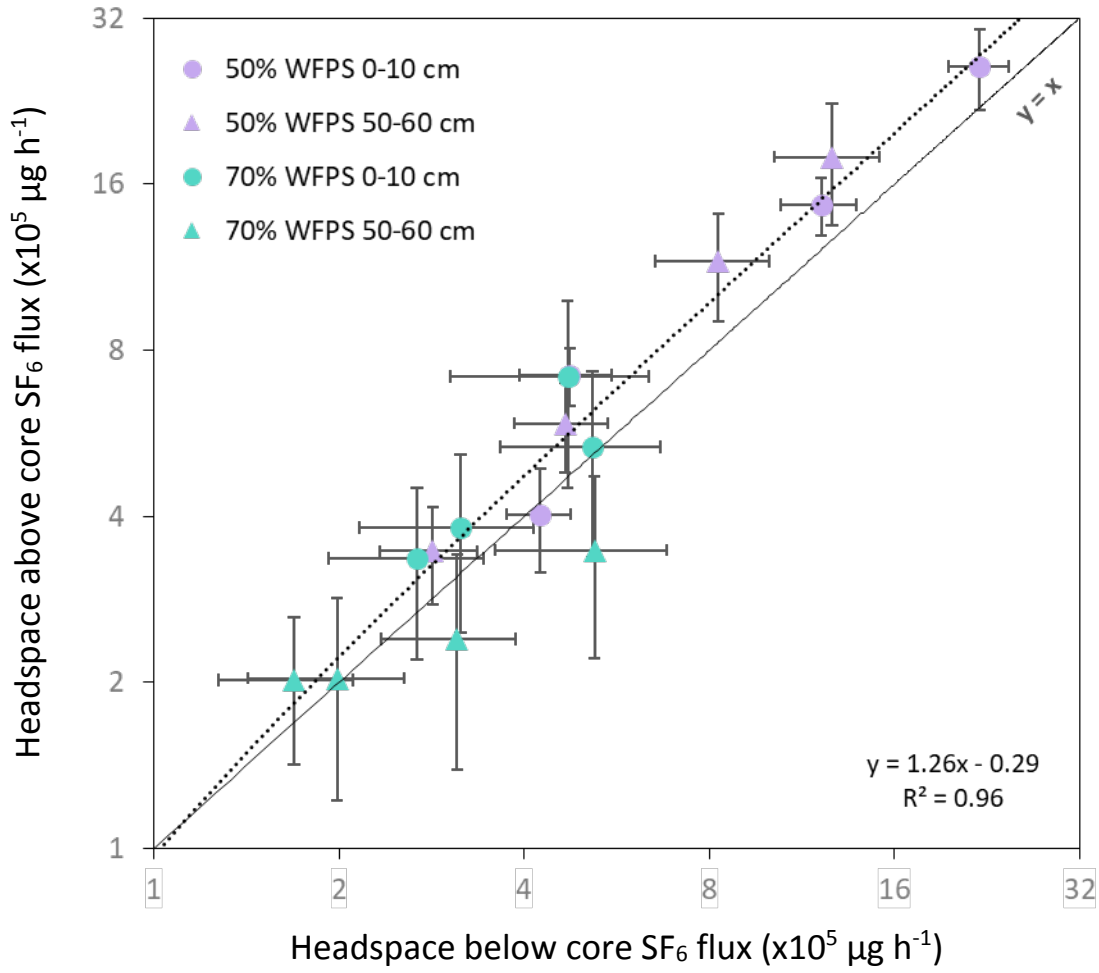

Fig. 2 The fluxes of SF_6 (means ± SEM; n = 6) from the headspace above versus the headspace below soil cores from the 0-10 and 50-60 cm soil depths at 50% and 70% WFPS. The dashed line represents the best fit for the flux data (R^2 = 0.96; y = 1.26x – 0.29) and the solid line represents the y = x. Note that the axes are logarithmic.

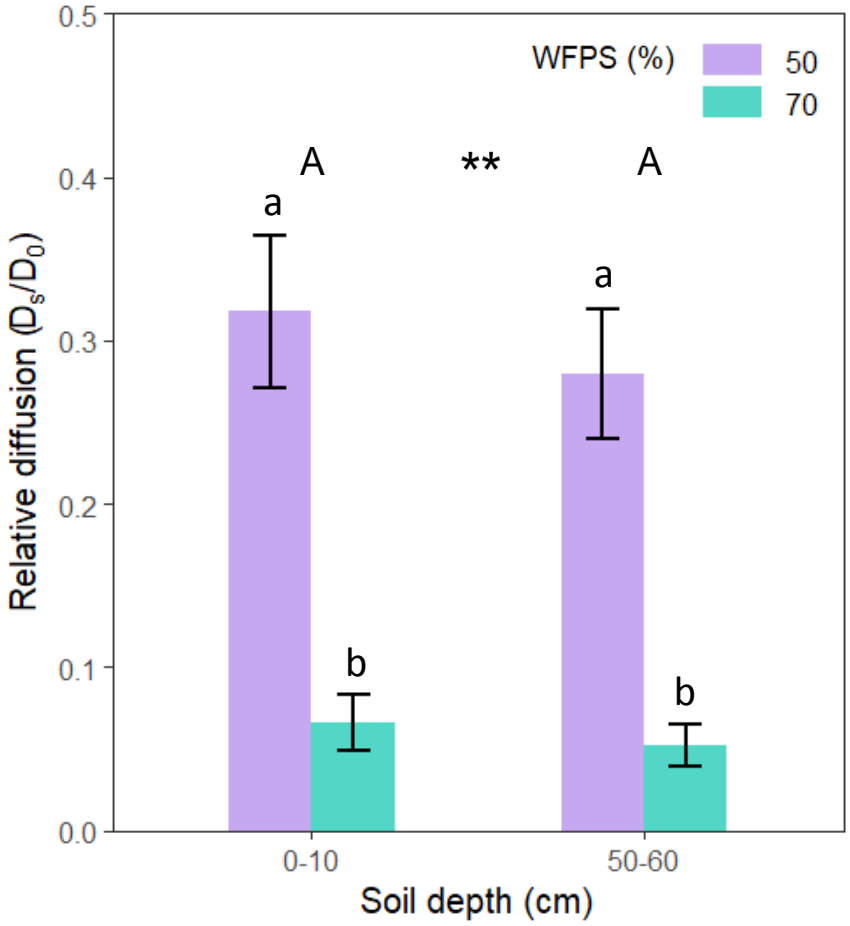

Fig. 3 The mean (± SEM) relative diffusivity (D_s/D_0) of intact top- and subsoil cores at 2 different levels of water-filled pore space (WFPS, %; n = 6). Different letters represent statistical difference of means between soil depths (upper-case) and between soil depth and WFPS (lower-case) at $p < 0.05$. Asterisks represent statistical difference in overall WFPS means at $p < 0.001$ (***); $p < 0.01$ (**); $p < 0.05$ (*) and $p > 0.05$ (-).

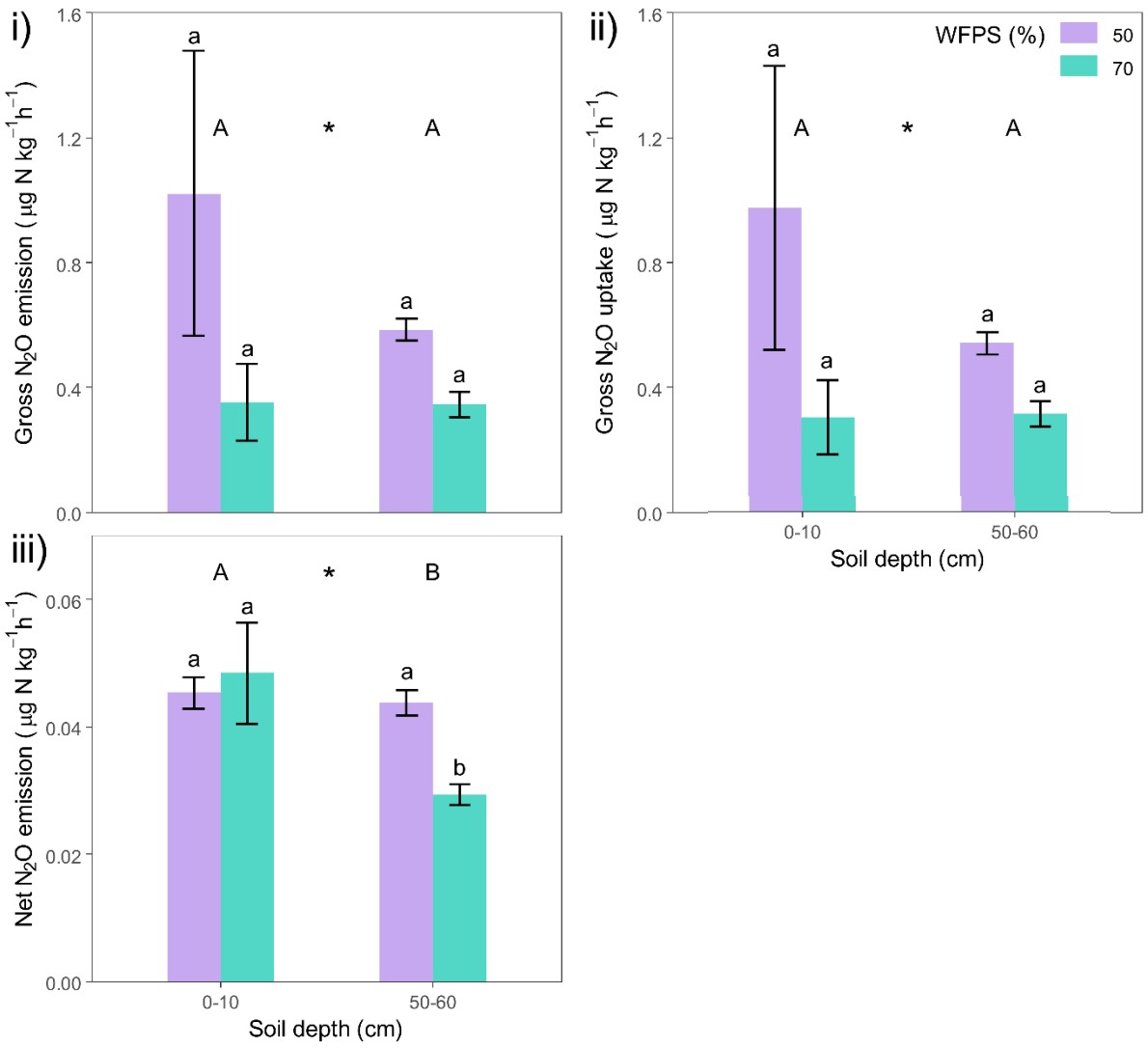

Fig. 4 The gross N_2O emission i); gross N_2O uptake ii), and; net N_2O emission iii) (means ± SEM; n = 6) in intact 0-10 and 50-60 cm soil cores at 50% and 70% WFPS measured by the ^{15}N-N_2O pool dilution method. Different letters represent statistical difference of means between soil depths (upper-case) and between soil depth and WFPS (lower-case) at $p < 0.05$. Asterisks represent statistical difference in overall WFPS means at $p < 0.001$ (***); $p < 0.01$ (**); $p < 0.05$ (*) and $p > 0.05$ (-).

Table 1. Properties of the Eutric Cambisol topsoil (0-10 cm) and subsoil (50-60 cm) used for the study. Values represent means ± SEM (*n* = 4) and values are expressed on a dry soil weight equivalent where appropriate.

Properties	Topsoil	Subsoil
	0 – 10 cm	50 – 60 cm
Sand (%)[†]	62.9 ± 0.7	67.2 ± 6.5
Silt (%)[†]	16.2 ± 1.3	14.9 ± 3.1
Clay (%)[†]	20.9 ± 1.0	17.9 ± 4.1
Dry bulk density (g cm^{-3})	1.11 ± 0.06	1.26 ± 0.04
Porosity (%)	55.7 ± 0.8	53.0 ± 3.5
Organic C (g C kg^{-1})	27.8 ± 1.3	7.4 ± 1.0
Total N (g N kg^{-1})	3.4 ± 0.1	1.5 ± 0.1
C:N ratio	8.1 ± 0.1	4.8 ± 0.3
pH_{H2O}	6.8 ± 0.06	6.8 ± 0.03
EC (µS cm^{-1})	1198 ± 126	657 ± 102
Extractable NH_4^+ (mg N l^{-1})	0.08 ± 0.02	0.09 ± 0.03
Extractable NO_3^- (mg N l^{-1})	41.1 ± 6.0	22.4 ± 5.2
Dissolved organic C (mg C l^{-1})	12.6 ± 1.3	4.3 ± 1.8
Dissolved organic N (mg N l^{-1})	4.9 ± 2.1	0.6 ± 0.4
Soil microbial biomass (mg C kg^{-1})	74.0 ± 3.7	42.9 ± 1.4

[†]data from Sanchez-Rodriguez et al., (in prep.), *n* = 4.